九州大学学術情報リポジトリ
Kyushu University Institutional Repository

Glial scar survives until the chronic phase by recruiting scar-forming astrocytes after spinal cord injury

田丸, 哲弥

https://hdl.handle.net/2324/6787512

出版情報：Kyushu University, 2022, 博士（医学）, 課程博士
バージョン：
権利関係：© 2022 Elsevier Inc. All rights reserved.

KYUSHU UNIVERSITY

Experimental Neurology 359 (2023) 114264

Contents lists available at ScienceDirect

Experimental Neurology

journal homepage: www.elsevier.com/locate/yexnr

Research paper

Glial scar survives until the chronic phase by recruiting scar-forming astrocytes after spinal cord injury

Tetsuya Tamaru [a], Kazu Kobayakawa [a,*], Hirokazu Saiwai [a], Daijiro Konno [b], Ken Kijima [a], Shingo Yoshizaki [c], Kazuhiro Hata [a], Hirotaka Iura [a], Gentaro Ono [a], Yohei Haruta [a], Kazuki Kitade [a], Kei-Ichiro Iida [a], Ken-Ichi Kawaguchi [a], Yoshihiro Matsumoto [a], Kensuke Kubota [d], Takeshi Maeda [d], Seiji Okada [e], Yasuharu Nakashima [a]

[a] Department of Orthopedic Surgery, Graduate School of Medical Sciences, Kyushu University, Fukuoka, Japan
[b] Department of Energy and Materials, Faculty of Science and Engineering Kindai University, Higashiosaka, Japan
[c] Department of Orthopedic Surgery, Kyushu University Beppu Hospital, Oita, Japan
[d] Department of Orthopedic Surgery, Spinal Injuries Center, Iizuka, Japan
[e] Department of Orthopedic Surgery, Graduate School of Medical Sciences, Osaka University, Suita, Japan

ARTICLE INFO

Keywords:
Spinal cord injury
Chronic phase
Glial scar
Reactive astrocyte
Scar-forming astrocyte
β_1-integrin

ABSTRACT

Spinal cord injury (SCI) causes reactive astrogliosis, the sequential phenotypic change of astrocytes in which naïve astrocytes (NAs) transform into reactive astrocytes (RAs) and subsequently become scar-forming astrocytes (SAs), resulting in glial scar formation around the lesion site and thereby limiting axonal regeneration and motor/sensory functional recovery. Inhibiting the transformation of RAs into SAs in the acute phase attenuates the reactive astrogliosis and promotes regeneration. However, whether or not SAs once formed can revert to RAs or SAs is unclear. We performed selective isolation of astrocytes from glial scars at different time points for a gene expression analysis and found that the expression of *Sox9*, an important transcriptional factor for glial cell differentiation, was significantly increased in chronic phase astrocytes (CAs) compared to SAs in the sub-acute phase. Furthermore, CAs showed a significantly lower expression of chondroitin sulfate proteoglycan (CSPG)-related genes than SAs. These results indicated that SAs changed their phenotypes according to the surrounding environment of the injured spinal cord over time. Even though the integrin-N-cadherin pathway is critical for glial scar formation, collagen-I-grown scar-forming astrocytes (Col-I-SAs) did not change their phenotype after depleting the effect of integrin or N-cadherin. In addition, we found that Col-I-SAs transplanted into a naïve spinal cord formed glial scar again by maintaining a high expression of genes involved in the integrin-N-cadherin pathway and a low expression of CSPG-related genes. Interestingly, the transplanted Col-I-SAs changed NAs into SAs, and anti-β_1-integrin antibody blocked the recruitment of SAs while reducing the volume of glial scar in the chronic phase. Our findings indicate that while the characteristics of glial scars change over time after SCI, SAs have a cell-autonomous function to form and maintain a glial scar, highlighting the basic mechanism underlying the persistence of glial scars after central nervous system injury until the chronic phase, which may be a therapeutic target.

1. Introduction

Spinal cord injury (SCI) disrupts communication within the nervous system, leading to the loss of the motor/sensory function (Van Middendorp et al., 2011; Mcdonald and Sadowsky, 2002). While rehabilitation can enhance partial spontaneous functional recovery, no effective treatment for chronic SCI patients has yet been developed (Hutson and Di Giovanni, 2019; Kobayakawa et al., 2019a; Shah et al., 2013). In the chronic phase of SCI, the glial scar acts as a physical barrier to regeneration and produces chondroitin sulfate proteoglycans (CSPGs), which function as a chemical barrier to regeneration (Tran et al., 2018; McKeon et al., 1991).

Astrocytes, the main cellular components of the glial scar, undergo a typical change of hypertrophy after SCI, showing process extension and

* Corresponding author.
E-mail address: kobayakawa.kazu.000@m.kyushu-u.ac.jp (K. Kobayakawa).

https://doi.org/10.1016/j.expneurol.2022.114264
Received 5 June 2022; Received in revised form 22 October 2022; Accepted 31 October 2022
Available online 3 November 2022
0014-4886/© 2022 Elsevier Inc. All rights reserved.

increased glial fibrillary acidic protein (GFAP) expression and presenting a characteristic morphology known as reactive astrocytes (RAs) (Hasel and Liddelow, 2021; Liddelow and Barres, 2017; Shinozaki et al., 2017). These RAs then overlap each other and subsequently transform into scar-forming astrocytes (SAs) that make a glial scar and inhibit the regeneration of axons, leading to limited recovery after SCI (Okada et al., 2006; Silver and Miller, 2004).

In contrast, in experiments that ablate reactive astrocytes or glial border astrocytes using transgenic mice or conditional ablation of astrocytes after SCI, increased leukocyte infiltration, progressive demyelination, and increased neuronal cell death were observed (Voskuhl et al., 2009; Sofroniew, 2005; Faulkner et al., 2004). In addition, experiments using mice specifically conditioned for reactive astrocytes showed no spontaneous axonal regeneration after severe SCI, either by blocking glial scar formation or by attenuation of scar astrocytes, or by the removal of astrocytes in the chronic phase (Anderson et al., 2016), suggesting diverse roles of astrocytes in the SCI pathology from the acute to the chronic phase.

We previously reported that the transformation of RAs into SAs could be stopped by blocking the integrin-N-cadherin pathway and that RAs could revert in retrograde to naïve astrocytes (NAs) by changing the extracellular environment (Hara et al., 2017). These findings suggest the possibility of therapy with an anti-integrin antibody targeting RAs in the acute/sub-acute phase. However, whether or not SAs in the chronic phase can change their morphology and gene expression phenotype by manipulating their extracellular environment is unclear.

In this study, we clarified the time course of changes in gene expression profiles in astrocytes after SCI by performing a selective gene expression analysis of NAs, RAs, SAs, and chronic-phase astrocytes (CAs) with laser microdissection (LMD). By manipulating the extracellular environment of scar-forming astrocytes *in vitro,* we investigated the change in the expression of SA marker genes and the reversibility of the morphological transformation characteristic of SAs. In particular, we focused on the influence of the integrin-N-cadherin pathway on the plasticity of SAs, as this pathway stops the transformation of RAs into SAs (Hara et al., 2017). Furthermore, we conducted transplantation of SAs into naïve spinal cord and analyzed the morphological/biological characteristics of transplanted astrocytes, indicating the dichotomic character of SAs regarding homeostasis and plasticity.

2. Materials and methods

2.1. Animals

We used 8- to 10-week-old C57BL/6 J mice (Japan SLC, Hamamatsu, Japan) and postnatal day 1–3 (P1–3) C57BL/6 J mice (Japan SLC, Hamamatsu, Japan) and CAG-EGFP mice (Japan SLC, Hamamatsu, Japan) in this study. All mice were housed in a temperature- and humidity-controlled environment on a 12-h light/dark cycle, with food and water available *ad libitum.*

All surgical procedures and experimental manipulations were approved by the Committee of Ethics on Animal Experimentation of the Faculty of Medicine, Kyushu University (A30–194-1). The experiments were conducted in accordance with the National Institutes of Health guidelines for the care and use of animals.

2.2. SCI induction

The mice were anesthetized with pentobarbital (75 mg/kg intraperitoneally) and subjected to a contusion injury (70 kdyn) at the 9th thoracic level using an Infinite Horizons Impactor (Precision Systems Instrumentation, Lexington, KY), as previously described (Yoshizaki et al., 2019). After the injury, the overlying muscles were sutured, and the skin was closed with wound clips. During recovery from anesthesia, the animals were placed in a temperature-controlled chamber until thermoregulation was re-established.

2.3. Primary astrocyte cultures and transplantation of astrocytes to the spinal cord

Purified primary astrocyte cultures were prepared from P1–3 C57BL/6 J mice or CAG-EGFP mice. As described in a previously reported article, we retrieved the brain cortices by grabbing the posterior end of the brain with fine forceps, performing a midline incision between the hemispheres, inserting a second set of forceps into the created groove, and peeling away the plate-like structure of the cortex from the brain without striatum (Schildge et al., 2013). We incubated the tissue in EBSS (Nacalai Tesque, Kyoto, Japan), 4 mg/ml DNase I (Sigma, Saint Louis, MO), and 20 U/ml papain (Worthington, Columbus, OH) at 37 °C for 40 min. We washed the tissue with a Trypsin inhibitor stock solution (Nacalai Tesque, Kyoto, Japan) and then gently triturated the tissue and added the single-cell suspension to a poly-D-lysine-coated T-75 Flask (Sigma, Saint Louis, MO) in an astrocyte culture medium (DMEM [Nacalai Tesque, Kyoto, Japan] containing 10% fetal bovine serum [FBS; Life Technologies, Carlsbad, CA], 0.2 mM GlutaMAX [Life Technologies, Carlsbad, CA], and 1% penicillin-streptomycin [Nacalai Tesque, Kyoto, Japan]). We replaced all volumes with fresh medium every three to four days to maintain the cultures. After 7 days in a humidified CO_2 incubator at 37 °C, we shook the T75 flask at 180 rpm for 30 min on an orbital shaker to remove microglia. We discarded the supernatant and added fresh astrocyte culture medium, then continued shaking the flask at 240 rpm for 6 h to remove oligodendrocyte precursor cells (OPCs), as described previously (McCarthy and de Vellis, 1980). The obtained astrocytes were used as serum-cultured primary astrocytes (PAs) as previously described (Hara et al., 2017). To activate PAs to IL-6-treated reactive astrocytes (IL-6-RAs), the astrocytes were stimulated with 50 ng/ml IL-6 (R&D Systems, Minneapolis, MN) and 200 ng/ml soluble IL-6 receptor (R&D Systems, Minneapolis, MN), as previously described (Hara et al., 2017). For the preparation of type I collagen-coated dishes, the dishes were incubated at 37 °C for 2 h with mouse type I collagen (50 μg/ml; Bio-Rad AbD Serotec, Hercules, CA), as described previously (Takahashi et al., 2015). To transform IL-6-RAs into Col-I-SAs, IL-6-RAs were detached from a dish and re-seeded on type I collagen-coated dishes, where they were incubated for 48 h (Hara et al., 2017). After washing Col-I-SAs three times with PBS, trypsin/EDTA (Nacalai Tesque, Kyoto, Japan) was added and the cells were stripped from the culture dish. We added the Col-I-SAs to the same volume of astrocyte medium as trypsin/EDTA, centrifuged at 1000 rpm 3 min at room temperature, and reseed them into Poly-D-Lysin-coated dishes, and immunohistological analysis and analysis of mRNA extraction were performed at 48 h after reseeded.

For transplantation of SAs, we used trypsin to detach Col-I-SAs from the dish after washing them three times with D-PBS(−); upon neutralizing the action of trypsin with medium containing FBS, we centrifuged the Col-I-SAs and discarded the supernatant. The resulting Col-I-SAs were resuspended in HBSS(−). The mice were anesthetized with pentobarbital (75 mg/kg intraperitoneally), and then a glass tip was inserted into naïve spinal cord, and Col-I-SAs (1×10^5) were injected at 0.5 μl/min using a stereotaxic injector (KDS 310; Muromachi Kikai, Tokyo, Japan). After the transplantation, the overlying muscles were sutured, and the skin was closed with wound clips. During recovery from anesthesia, the animals were placed in a temperature-controlled chamber until thermoregulation was re-established.

2.4. Administration of antibody against integrin β_1

As previously described (Hara et al., 2017), mice transplanted EGFP-positive Col-I-SAs with an injection of 1 μg of monoclonal antibody against integrin β_1 (anti-β_1 Ab; BD Pharmingen, San Diego, CA, 555003) at the area where the EGFP-positive SAs were transplanted using a stereotaxic injector (KDS 310, Muromachi Kikai, Tokyo, Japan) every 2 d from 2 to 12 days post transplantation. Control mice were given an equivalent amount of isotype control antibody (control Ab; BD

Pharmingen, San Diego, CA, 553958). Mice with SCI received an injection of the equivalent amount of anti-β_1 Ab at the epicenter using a stereotaxic injector every 2 d from 14 to 26 days-post injury. Control mice were given an equivalent amount of isotype control antibody. For *in vitro* blocking of collagen–integrin signaling, anti-β_1 Ab or control Ab was added at 1 μg/ml, and immunohistological analysis and analysis of mRNA extraction were performed at 24 h after antibody administration.

2.5. Administration of N-cadherin neutralizing antibody

We added 10 μg of neutralizing monoclonal antibody against N-cadherin (N-cadherin nAb; Sigma-Aldrich, Saint Louis, MO, C3865) or equivalent amount of isotype control IgG (control IgG; BioXCell, Lebanon, NH, BE0083) *in vitro* culture of SAs, and immunohistological analysis was performed 24 h after antibody administration.

2.6. LMD

As previously described (Kobayakawa et al., 2019a, 2019b), fresh naïve, injured spinal cords, and naïve spinal cords which transplanted CAG-EGFP SAs were immediately frozen in dry ice/hexane and stored in a deep freezer at −80 °C. The tissues were sectioned into 16-μm slices using a cryostat (Leica Microsystems, Wetzlar, Germany) at −20 °C and mounted on polyethylene naphthalate (PEN) membrane slides (Leica Microsystems, Wetzlar, Germany). The sections were then fixed in ice-cold acetone for 3 min and subsequently stained with primary antibodies in PBS(−) at room temperature for 5 min followed by washing in PBS(−) for 1 min. The sections then were stained with secondary antibodies in PBS(−) at room temperature for 5 min.

We use the primary antibody Rabbit Anti-GFAP Antibody (1:50; rabbit; Z0334, Dako, Santa Clara, CA) and secondary antibody Goat anti-rabbit Alexa Fluor 488 Antibody (1:250; Jackson ImmunoResearch, West Grove, PA).

GFAP-positive astrocytes or EGFP-positive SAs were dissected with an LMD 6500 system (Leica Microsystems, Wetzlar, Germany) and were transferred by gravity into a microcentrifuge tube cap placed directly beneath the section. The tube cap was filled with 75 μl of buffer RLT (Qiagen, Venlo, The Netherlands). For each sample, 1000 cells were dissected from one series of sagittal sections and subjected to RNA extraction. Total RNA was isolated using the RNeasy Mirco kit (Qiagen, Venlo, The Netherlands). An excellent RNA quality as well as no contamination with other cell types was confirmed with a Bioanalyzer and PCR analyses of the collected samples of astrocytes (Fig. S1), as previously described (Hara et al., 2017).

2.7. Reverse transcription polymerase chain reaction (RT-PCR)

Total RNA of astrocytes selectively recovered using LMD was extracted using the RNeasy Mirco kit (Qiagen, Venlo, the Netherlands). For cDNA synthesis, a reverse transcription reaction was performed using SuperScript VILO cDNA Synthesis Kit (Invitrogen, Waltham, MA, USA). The cDNA was mixed with KOD One (TOYOBO, Osaka, Japan). PCR was performed using a T100 thermal cycler (Bio-Rad, Hercules, CA, USA), and the products were detected by electrophoresis.

2.8. Quantitative reverse transcription polymerase chain reaction (Quantitative PCR)

Total RNA was isolated from the astrocytes obtained from spinal cord tissue using the RNeasy Mini kit (Qiagen, Venlo, The Netherlands). For cDNA synthesis, a reverse transcription reaction was performed using SuperScript VILO cDNA Synthesis Kit (Invitrogen, Waltham, MA). Quantitative real-time PCR was performed using primers specific to the genes of interest (Table 1) and KOD SYBR qPCR Mix (TOYOBO, Osaka, Japan). The data were normalized to the expression of glyceraldehyde-3-phosphate dehydrogenase. Real-time PCR was conducted using a CFX Connect Real-Time PCR Detection System (Bio-Rad, Hercules, CA).

2.9. Histopathological examinations

After animals were anesthetized and transcardially fixed with 4% paraformaldehyde (PFA; Millipore, Burlington, MA), the spinal cord was removed, dehydrated, and embedded in an optimal cutting temperature compound (Sakura Finetek Japan, Tokyo, Japan). The sections were mounted on MAS-coated slide glasses (Matsunami Glass, Kishiwada, Japan). On the other hand, the astrocytes cultured *in vitro* were washed three times with PBS, and fixed for 15 min in 4% PFA/PBS at room temperature. After washing three times with PBS, these sections and cells were used for the following immunofluorescent staining. Then the sections were stained with the following antibodies in blocking solution at 4 °C overnight: GFAP (1:500; rabbit; Dako, Santa Clara, CA; Z0334), GFAP (1:500; rat; Life Technologies, Carlsbad, CA; 130,300), N-cadherin (1:1000; mouse; BD Transduction Laboratories, San Diego, CA; 610,921), GAP43 (1:500; rabbit; Novus Biologicals, Centennial, CO; NB300–143).

The primary antibodies were visualized with the secondary antibodies conjugated to Alexa 488, 568, 647 (1:1000; Jackson ImmunoResearch, West Grove, PA). The nucleus was visualized with Hoechst 33258 (1:1000; Invitrogen, Waltham, MA). All images were captured using a BZ-X700 digital microscope system (Keyence, Osaka, Japan) or BX51 (Olympus, Tokyo, Japan) epifluorescence microscope equipped with a DP71 Camera (Olympus, Tokyo, Japan).

To calculate the percentage of cells with overlapping astrocyte legs, the percentage of GFAP- and Hoechst-positive cells with overlapping astrocyte legs in one field of view observed under a microscope was calculated.

2.10. Quantitative analyses for immunohistolog

For the quantification of the GFAP positive area, we obtained sagittal sections at 100 μm intervals from the injured spinal cord in each mouse. The GFAP positive area which was 500 μm from the rostral and the

Table 1
Primers used for RT-PCR.

Gene symbol	Accession number	5'-Forward primer-3'	5'-Reverse primer-3'
Cd11b	NM_001082960.1	AAGCAGCTGAATGGGAGGAC	TAGATGCGATGGTGTCGAGC
Cdh2	NM_007664.4	TACGCAGCTGGTTGCAGATAAAGG	TCTGCACTCCTCCATAGTCTATGC
Csgalnact1	NM_001252623.1	CTTGAGACAGTCTTGTCACAGAGC	CAGTCCTTAGATCAGATCTCCAGG
Cx3cr1	NM_009987.4	CTTCCCATCTGCTCAGGACCTC	CCAGACCGAACGTGAAGACGA
Gapdh	NM_008084.3	GACTTCAACAGCAACTCCCACTCT	GGTTTCTTACTCCTTGGAGGCCAT
Mbp	NM_001025251.2	TCTTTAAGCTGGGAGGAAGAGAC	GCTCCACGGGATTAAGAGAGG
Neun	NM_001039167.1	CCGTTCTGCAAACAGAGAGC	GTCCCAGCAATGGGCTGT
Pdgfra	NM_001083316.2	ATCGGCCAGCCTCCTACAAG	GGTCCCGGTGGACACAATTTTT
Pcan	NM_001081306.1	TAATGGTGCAGCTTTGCCTGATGG	GCAGCAGAATGAGTTACTGTCAGG
Slit2	NM_001291227.1	CGTCTCTAGAAGCTTCTAGCTTCG	TGTAGGGGGAGCTTTAGTACAAGC
Sox9	NM_011448.4	GAAGGTAACGATTGCTGGGATTCC	CGTCCTCCATGTTAACTCTGAAGG
Xylt1	NM_175645.3	CAGTGAAGATTCTCCATCACTGGG	TCTGGAAACTCTGCTCCATGTAGG

caudal of the epicenter was measured using the ImageJ software program (National Institutes of Health, Bethesda, MD). For the quantification of the astrocytes with process overlap, we randomly selected 20 cells in each sample and measured the astrocyte cell diameter or proportion of cells with overlapping neighboring astrocytic processes using the ImageJ software program (US National Institutes of Health). For the quantification of the astrocytes next to the transplanted SAs, we obtained sagittal sections at 32 μm intervals from the transplanted spinal cord. EGFP^{-}/GFAP^{+}/N-cadherin^{+} cells contacting with EGFP^{+}/GFAP^{+}/N-cadherin^{+} SAs were counted using the BZII-Analyzer measurement software program (Keyence, Osaka, Japan). For the quantification of the SAs after administration of anti-β_1 Ab or control Ab, we obtained sagittal

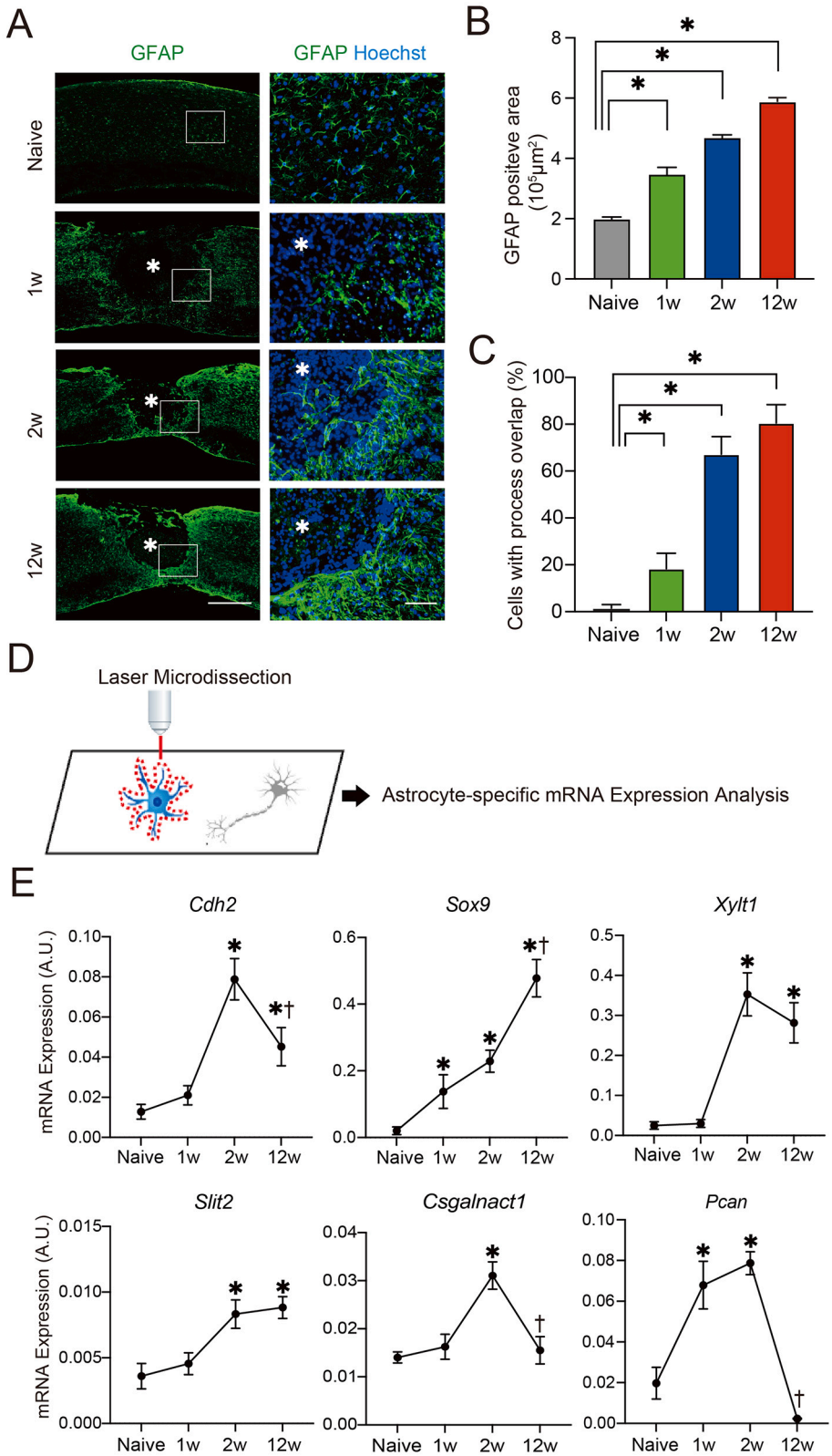

Fig. 1. The glial scar formed at 2 wpi had different characteristics from that at 12 wpi. (A) Representative images of immunofluorescent staining of the spinal cord with GFAP (green) and Hoechst (blue) in the naïve spinal cord and injured cord at 1, 2, and 12 wpi. The asterisks indicate the epicenters of the injured spinal cord. Inset: High-magnification image. Scale bars, 500 μm (Left), 200 μm (right). The images shown are representative of eight mice per time point per group. (B) The quantitative analysis of the GFAP-positive area (n = 8 mice per group) (C) The percentage of astrocytes with overlapping of neighboring astrocytic processes in naïve or injured spinal cord (n = 8 mice per group). (D) A schematic representation of the selective isolation of GFAP-positive astrocytes using LMD for the cell-type specific gene expression analysis. (E) The quantitative analysis of the mRNA expression of SA-related genes in astrocyte selectively isolated from naïve and injured cord at 1, 2, and 12 wpi. Expression levels were expressed in arbitrary units (AU) relative to GAPDH (n = 6 mice per group). An ANOVA with the Tukey-Kramer *post hoc* test: *P < 0.05. † indicates significance between astrocytes isolated from injured cords of 2 and 12 wpi. n.s., not significant. Data represent the mean ± s.e.m. (For interpretation of the references to colour in this figure legend, the reader is referred to the web version of this article.)

sections at 100 μm intervals from the injured spinal cord in each mouse. GFAP$^+$/N-cadheirn$^+$ SAs which were 500 μm rostral or caudal from the epicenter were counted using the BZII-Analyzer measurement software program (Keyence, Osaka, Japan). The GAP43-positive area was measured at 2 mm rostral from the center of injury using the BZII-Analyzer measurement software program (Keyence, Osaka, Japan).

2.11. Statistical analyses

Statistical evaluations were performed with Wilcoxon's rank-sum test. An ANOVA with the Tukey-Kramer post-hoc test was used for multiple comparisons between groups. In all statistical analyses, significance was defined as $p < 0.05$. In graphs, data are presented as the mean ± SEM. All statistical analyses were performed using the Graph Pad Prism software program, version 9.1.2 (GraphPad Software Inc., San Diego, CA).

3. Results

3.1. The astrocytes in the glial scar changed their gene expression profile over time

After SCI, astrocytes surrounding the lesion area become reactive. They underwent morphological changes, such as hypertrophy, process extension, and the increased expression of GFAP, showing the typical morphology of RAs at 1 week post-injury (wpi) (Fig. 1A). At 2 wpi, astrocytes around the epicenter overlapped their processes and transformed into SAs, forming the glial scar (Fig. 1A). The GFAP-positive area expanded over time (Fig. 1B). To quantify the morphological differences among astrocytes at different time points after SCI, we counted the astrocytes with overlapping processes between neighboring astrocytes around the epicenter and found that process overlap significantly increased over time (Fig. 1C and Fig. S1C). These results indicated that the glial scar persisted until the chronic phase (12 wpi) with increased process overlap of astrocytes.

We previously reported that SAs showed a significantly higher expression of *Cdh2* (encoding N-cadherin), *Sox9,* and CSPG-related genes (*Xylt1, Csgalanact1, Pcan, and Slit2*) than NAs and RAs (Hara et al., 2017). However, whether or not the gene expression properties of astrocytes at 12 wpi (in CAs), are the same as those of SAs at 2 wpi remains unclear. To clarify this issue, we isolated astrocytes from the naïve spinal cord and lesion area of the injured spinal cord at 1, 2, and 12 wpi using LMD (Fig. 1D) and investigated the expression of characteristic genes of SAs, such as *Cdh2*, *Sox9*, *Xylt1*, *Slit2, Csgalanact1,* and *Pcan*. Interestingly, while the *Sox9* expression in CAs was significantly elevated compared to that in SAs, we detected a significantly reduced expression of *Cdh2*, *Csgalanact1*, and *Pcan* in CAs compared with that in SAs (Fig. 1E). Contrary to expectations that the scars would retain the same properties, these results indicated that astrocytes in the glial scar changed their phenotypes according to the surrounding environment of the injured spinal cord over time, suggesting the importance of understanding the plasticity of astrocytes in the glial scar.

3.2. SAs did not revert to RAs/NAs based on changes in the environment in vitro

It has long been considered that the sequential phenotypic changes in astrocytes after SCI are unidirectional and irreversible. However, we recently demonstrated that RAs were regulated by the surrounding environment and could be reverted to NAs (Hara et al., 2017). In the usual course of SCI, RAs eventually become SAs, which mainly compose the glial scar. Since the glial scar prevents axonal regeneration by producing axonal growth inhibitors, redirecting SA morphology towards RAs or NAs may have the potential to promote functional recovery. Therefore, to confirm whether or not SAs could be reverted to RAs or NAs by changing the surrounding environment, we first prepared IL-6-treated reactive astrocytes (IL-6-RAs) from the serum-cultured primary astrocytes (PAs) harvested from neonatal mice from P1 to P3 by adding IL-6 and soluble IL-6 receptor (Fig. 2A).

These IL-6-RAs exhibited the same phenotypes as *in vivo* RAs, including hypertrophy, process extension, and increased GFAP expression (Fig. 2B). We then cultured these IL-6-RAs on type I collagen-coated dishes to obtain collagen-I-grown scar-forming astrocytes (Col-I-SAs), which exhibited the same phenotypes as *in vivo* SAs (Fig. 2A) as previously described (Hara et al., 2017). These Col-I-SAs showed a significantly higher expression of SA marker genes than PAs (Fig. 2C) and had a flattened morphology clearly different from IL-6-RAs and PAs (Fig. 2B). Since type I collagen induces the transformation of RAs into SAs, we speculated that eliminating the effect of type I collagen led to the morphological changes in SAs.

To verify this hypothesis, we reseeded Col-I-SAs cultured with type I collagen-coated dish into Poly-D-Lysin-coated dishes (Fig. 2D). After reseeding, the Col-I-SAs maintained their flattened morphology and N-cadherin expression (Fig. 2E). To compare the expression of SA marker genes of Col-I-SAs on type I collagen-coated dishes to those on Poly-D-Lysin-coated dishes, we performed quantitative PCR for *Cdh2*, *Sox9*, *Xylt1*, *Csgalanact1*, *Pcan*, and *Slit2* and found that the SA maker gene expression was similar between SAs on type I collagen-coated and Poly-D-Lysin-coated dishes (Fig. 2F). These results suggested that once type I collagen had induced the transformation of IL-6-RAs into Col-I-SAs, the elimination of the type I collagen-induced signal transduction failed to revert Col-I-SAs to IL-6-RAs/PAs.

3.3. Pharmaceutic inhibition of the integrin-N-cadherin pathway did not revert SAs to RAs/NAs in vitro

We previously reported that integrins, major cell receptors for extracellular matrix protein, directly mediated the RA-type I collagen interaction and induce the transformation of RAs into SAs. In addition, blocking the integrin-mediated RA-type I collagen interaction by anti-β_1 integrin Ab treatment inhibited the transformation of RAs into SAs in the type I collagen-coated dish (Hara et al., 2017). Therefore, we hypothesized that SAs could be reverted to RAs or NAs by administering anti-β_1 integrin antibodies to *in vitro*. However, the morphology of Col-I-SAs and the expression of N-cadherin, a hallmark of SA, remained unchanged after anti-β_1 integrin antibody treatment (Fig. 3A). We further examined the effect of the β_1 integrin antibody treatment on the expression of SA marker genes, but β_1 integrin antibody had no significant effect on the expression of SA marker genes (Fig. 3B).

SAs are the main component of glial scars, and N-cadherin-mediated adhesion of SAs play a major role in glial scar formation (Nathan and Li, 2017). In this study, we confirmed that N-cadherin expression was significantly increased in Col-I-SAs compared with IL-6-RAs or PAs (Fig. 2C). Since astrocyte-specific knockout of N-cadherin results in impairment of astrogliosis (Kanemaru et al., 2013), we administered N-cadherin–neutralizing antibody to Col-I-SAs to verify whether or not the characteristics of SAs were affected by the antibody. Even after N-cadherin-neutralizing antibody treatment, the morphology of SA remained unchanged compared to the control antibody-treated group, and N-cadherin expression was also observed. (Fig. 3C). The expression of SA marker genes in Col-I-SAs with N-cadherin-neutralizing antibody treatment showed no significant difference from the expression in those with control IgG treatment (Fig. 3D).

Based on these results, we concluded that the morphological characteristics and gene expression profiles of Col-I-SAs were highly robust to pharmaceutical treatments, focusing on type I collagen, integrin, and N-cadherin.

3.4. SAs induce surrounding naïve astrocytes to become SAs

Even though Col-I-SAs did not change into IL-6-RAs/PAs by inhibiting the integrin-N-cadherin pathway, we suspected that there might be

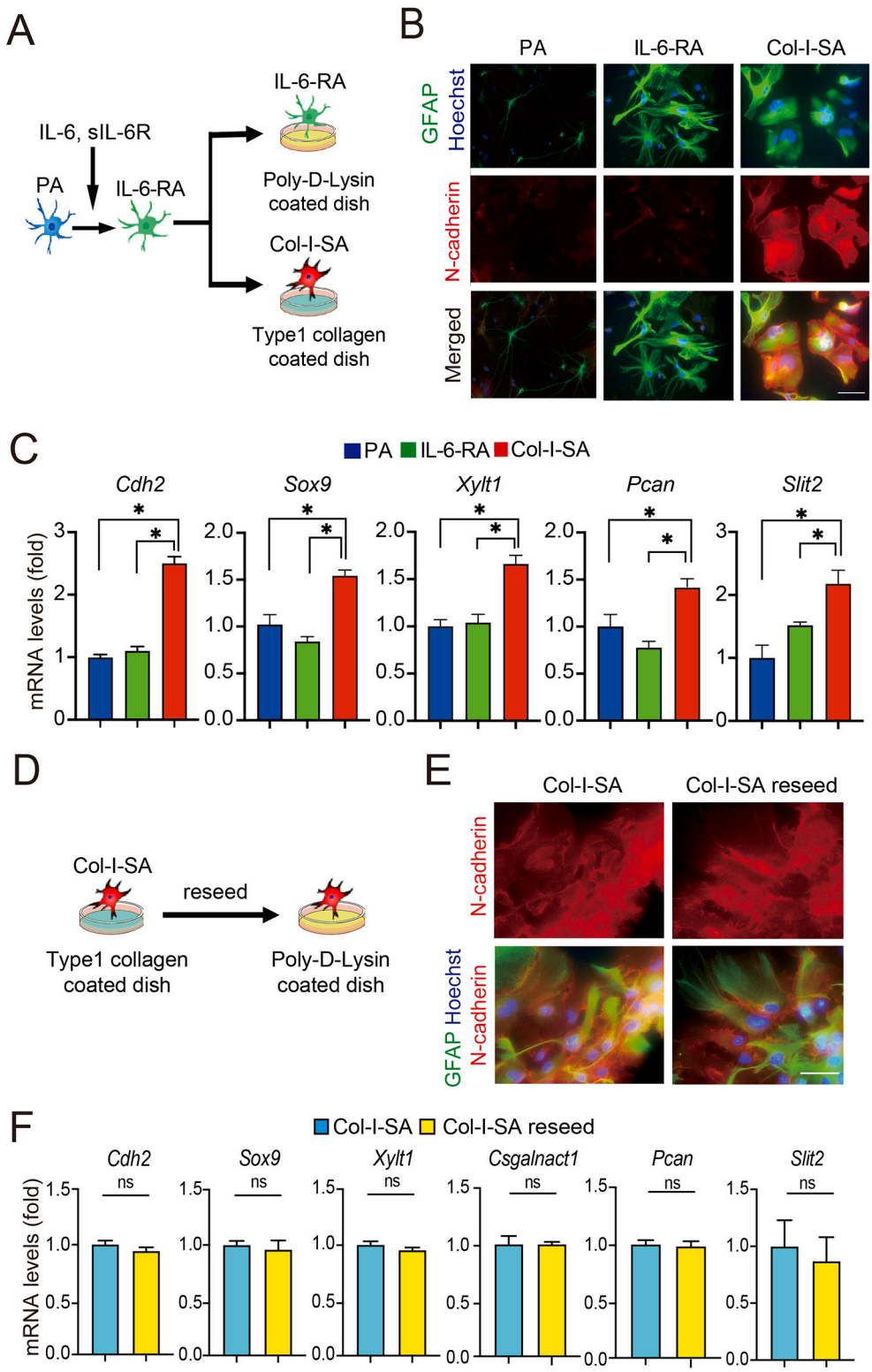

Fig. 2. Eliminating type 1 collagen signaling did not revert SAs to RAs or NAs *in vitro*. (A) The protocol for obtaining IL-6-RAs and Col-I-SAs from PAs. PAs treated with IL-6 and sIL-6R changed to IL-6-RAs. IL-6-RAs reseeded in Poly-D-Lysin-coated dishes retained the characteristic morphological features of RAs, while those reseeded in Type I collagen-coated dishes changed into Col-I-SAs. (B) Representative images of immunofluorescent staining of PAs, IL-6-RAs, and Col-I-SAs with GFAP (green), N-cadherin (red), and Hoechst (blue) *in vitro*. (C) Quantification of the mRNA expression of SA-related genes in PAs, IL-6-RAs, and Col-I-SAs ($n = 6$ wells per group). Gene expression was normalized to that of PAs. (D) Col-I-SAs provided as shown in (A) were reseeded from Type I collagen-coated dishes to Poly-D-Lysin-coated dishes. (E) Representative images of immunofluorescent staining of Col-I-SAs and reseeded Col-I-SAs with GFAP (green), N-cadherin (Red), and Hoechst (blue) *in vitro*. Scale bars, 50 μm. (F) Quantification of the mRNA expression for SA-related genes in Col-I-SAs and reseeded Col-I-SAs ($n = 6$ wells per group). Gene expression was normalized to that of Col-I-SAs. An ANOVA with the Tukey-Kramer *post hoc* test (C) and Wilcoxon rank-sum test (F): $^*P < 0.05$. n.s., not significant. Data represent the mean ± s.e.m. (For interpretation of the references to colour in this figure legend, the reader is referred to the web version of this article.)

other factors that affect SA plasticity. We previously reported that RAs had plasticity, depending on the surrounding environment, by demonstrating that RAs transformed into NAs when they were transplanted into naïve spinal cord (Hara et al., 2017). Therefore, we transplanted Col-I-SAs generated from CAG-EGFP mice into naïve spinal cords of wild-type (WT) mice to verify whether or not a different surrounding environment would affect the characteristics of SAs (Fig. 4A). Interestingly, the transplanted SAs adhered to each other and formed a glial scar with abundant N-cadherin expression in the environment of the uninjured spinal cord, suggesting that SAs have a cell-autonomous function to form a glial scar (Fig. 4B).

Next, using LMD, we selectively isolated EGFP-positive SAs and performed a quantitative gene expression analysis (Fig. 4C). There was no significant difference in the gene expression of *Cdh2*, *Sox9*, and *Slit2* between transplanted SAs at 2 or 4 weeks (14 or 28 d) after transplantation into the uninjured spinal cord and those at the day of

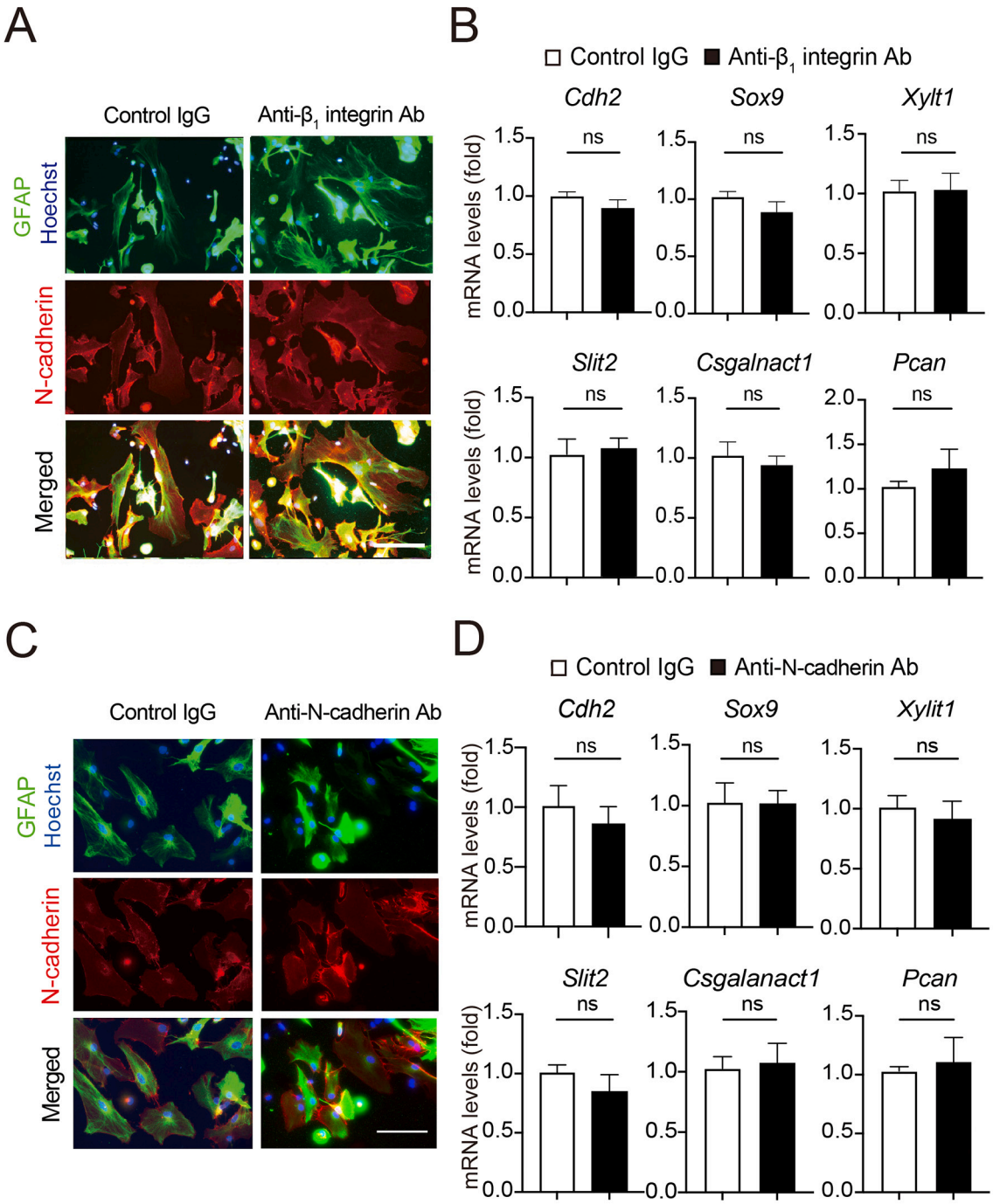

Fig. 3. Pharmaceutic inhibition of the β_1 integrin-N-cadherin pathway did not revert SAs to RAs or NAs *in vitro*. (A) Representative images of immunofluorescent staining of Col-I-SAs with anti-β_1-integrin antibody or control antibody. GFAP (green), N-cadherin (red), and Hoechst (blue). Scale bar, 50 μm. (B) Quantification of the mRNA expression for SA-related genes in Col-I-SAs with anti-β_1-integrin antibody or control antibody. ($n = 6$ wells per group). Gene expression was normalized to Col-I-SAs with control IgG. (C) Representative images of immunofluorescent staining of Col-I-SAs with anti-N-cadherin antibody or control antibody with GFAP (green), N-cadherin (red), and Hoechst (blue). Scale bar, 50 μm. (D) Quantification of the mRNA expression for SA-related genes in Col-I-SAs with anti-N-cadherin antibody or control antibody. ($n = 6$ wells per group). Gene expression was normalized to Col-I-SAs with control antibody. Wilcoxon rank-sum test: $^*P < 0.05$. n.s., not significant. Data represent the mean ± s.e.m. (For interpretation of the references to colour in this figure legend, the reader is referred to the web version of this article.)

transplantation (0 d) (Fig. 4D and Fig. S2A—B). This result suggests the robustness of the integrin/N-cadherin pathway of SAs, which might be the mechanism underlying how SAs maintain their morphology over time. In contrast, the expression of CSPG-related genes, such as *Xylt1*, *Csgalanact1*, and *Pcan*, in transplanted SAs was significantly decreased at 14 d (Fig. 4D and Fig. S2B), showing the possibility of environment-dependent plasticity in SAs.

While we were observing SAs transplanted in naïve spinal cords, we noticed an interesting fact that EGFP-negative host astrocytes grew in size and expressed N-cadherin at 14 days after transplantation (Fig. 4B, arrowheads), suggesting that the transplanted SAs might change the host naïve astrocytes to SAs.

Next, we selectively isolated host astrocytes adjacent to the transplanted SAs using LMD and performed a gene expression analysis

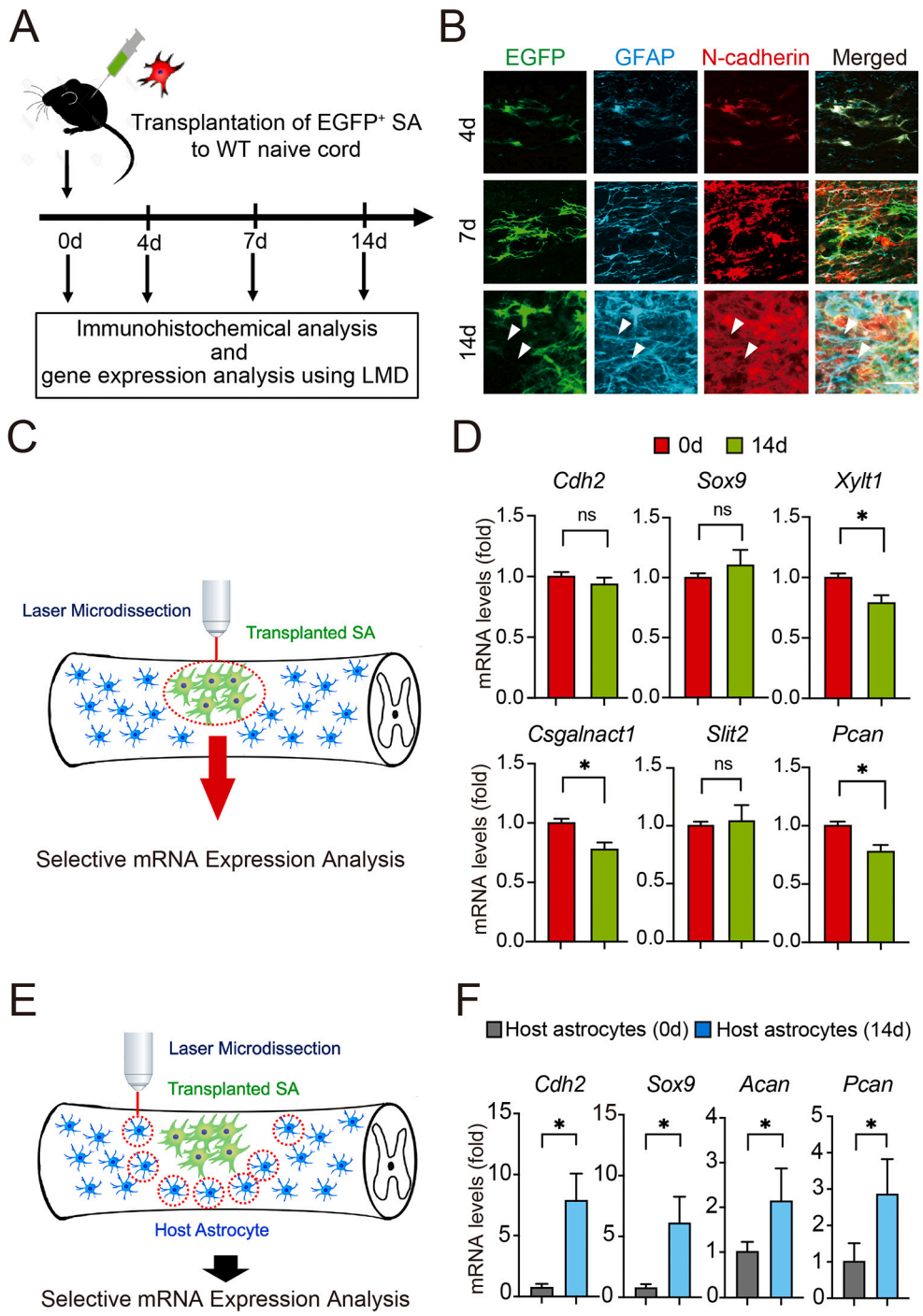

Fig. 4. SAs transplanted into naïve spinal cord changed host NAs to SAs. (A) EGFP-positive Col-I-SAs were provided from CAG-EGFP neonatal mice using the method shown in Fig. 2A. EGFP-positive Col-I-SAs were transplanted into naïve spinal cord of WT mice. (B) Representative images of immunofluorescent staining of transplanted cells with GFAP (green), N-cadherin (red), and Hoechst (blue) at 4, 7, and 14 days of transplantation. Scale bar, 100 μm. (C) A schematic representation of the selective isolation of EGFP-positive transplanted astrocytes using LMD for a cell-type specific gene expression analysis. (D) Quantification of the mRNA expression for SA-related genes in SAs on the day of transplantation (0 d) and at 14 days post-transplantation (14 d) ($n = 6$ mice per group). Gene expression was normalized to 0 d. (E) A schematic representation of the selective isolation of EGFP-negative/GFAP-positive astrocytes surrounding transplanted astrocytes using LMD. (F) Quantification of the mRNA expression for SA-related genes in host astrocytes surrounding EGFP-positive SAs on the day of transplantation (0 d) and at 14 days post-transplantation (14 d) (n = 6 mice per group). Wilcoxon rank-sum test: $^*P < 0.05$. n.s., not significant. Data represent the mean ± s.e.m. (For interpretation of the references to colour in this figure legend, the reader is referred to the web version of this article.)

(Fig. 4E). Surprisingly, host astrocytes at 14 or 28 days after transplantation (14 or 28 d) showed a significantly elevated expression of genes that characterize SAs, such as *Cdh2, Sox9, Acan* and *Pcan*, compared to those on the day of transplantation (0 d) (Fig. 4F and Fig. S2C). These results indicated that SAs have robustness to maintain themselves as SAs, even in uninjured spinal cords, and that SAs can change adjacent astrocytes to SAs, which may be a mechanism underlying how the glial scar persists until the chronic phase.

3.5. β_1 integrin antibody treatment in the chronic phase inhibits recruitment of SAs

To examine whether or not recruitment of SAs from astrocytes around transplanted SAs occurred *via* the β_1 integrin-N-cadherin axis, we administered anti-β_1 integrin antibody after transplantation of SAs *in vivo* (Fig. 5A). While astrocytes around transplanted SAs without anti-β_1 integrin antibody transformed to N-cadherin-positive SAs, blocking β_1 integrin inhibited the recruitment of SAs from EGFP-negative host astrocytes (Fig. 5B and C). These results suggest that SAs in the chronic phase after SCI also recruit SAs *via* the β_1 integrin-N-cadherin axis. Therefore, we next injected anti-β_1 integrin antibody into spinal cord from 14 to 28 days after SCI (Fig. 5D) and found significantly decreased numbers of GFAP/N-cadherin-positive SAs (Fig. 5E and F). Moreover, we next examined whether reduction of SAs with β_1 integrin antibodies affect axonal regeneration. Immunohistochemical analysis of GAP43 expression in the spinal cord revealed significantly increased

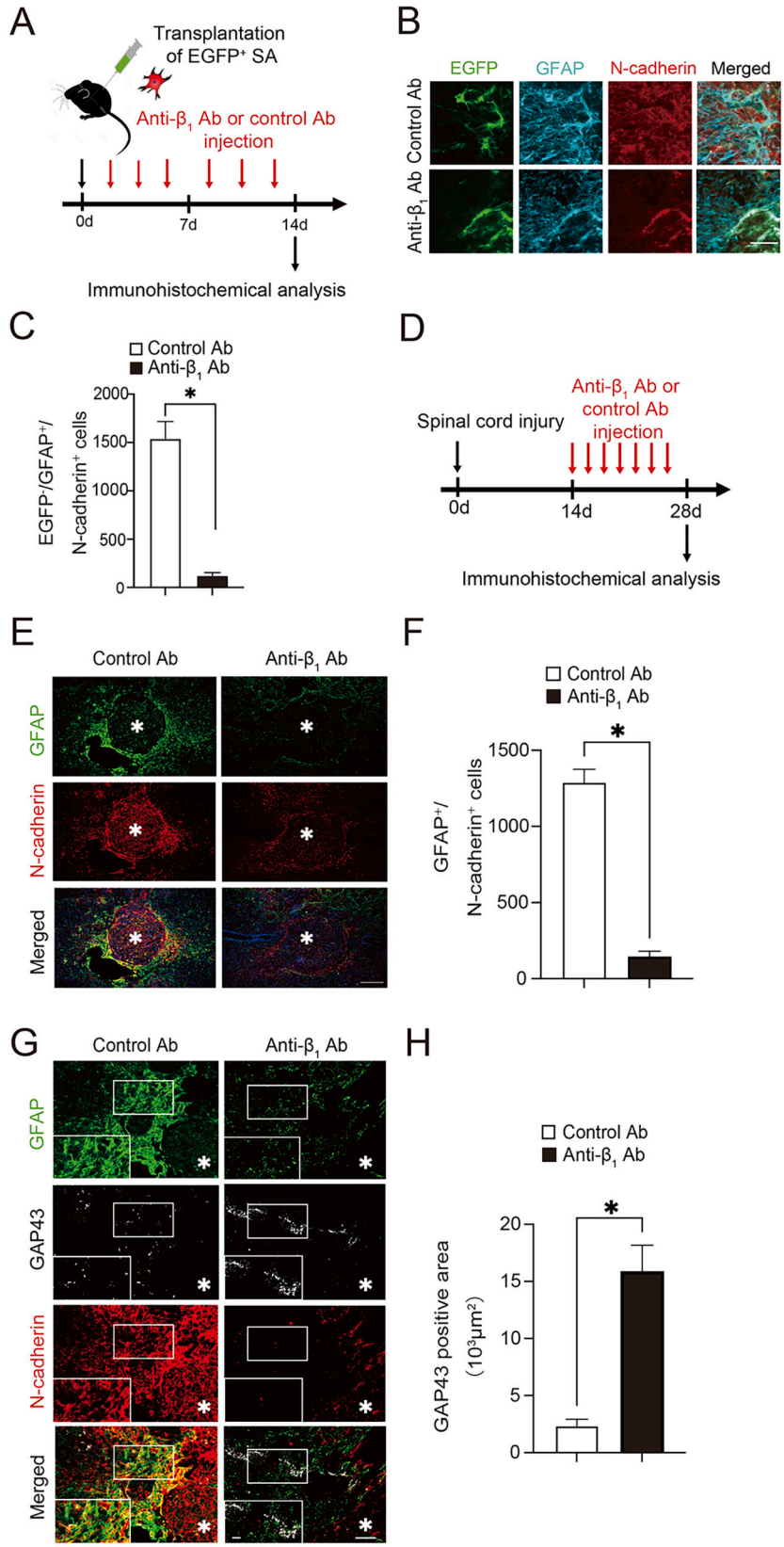

Fig. 5. Anti-β_1 integrin antibody blocked recruitment of SAs. (A) The experimental protocol of anti-β_1 integrin antibody after transplantation of SAs into naïve spinal cord. (B) Representative images of immunofluorescent staining of transplanted cells with EGAP (green), GFAP (blue), N-cadherin (red) at 14 days after transplantation. Scale bar, 100 μm. (C) Quantification of GFP-negative/GFAP-positive/N-cadherin-positive CAs derived from host astrocytes with/without anti-β_1 integrin antibody at 14 days after transplantation (n = 6 mice per group). (D) The experimental protocol of injection of anti-β_1 integrin antibody into spinal cord after SCI. (E) Representative images of immunofluorescent staining of spinal cord with/without anti-β_1 integrin antibody after SCI. The asterisks indicate the epicenters of the injured spinal cord. Scale bar, 500 μm. (F) Quantification of GFAP-positive/N-cadherin-positive CAs at 28 dpi (n = 6 mice per group). (G) Representative images of immunofluorescent staining of spinal cord with/without anti-β_1 integrin antibody after SCI. The asterisks indicate the epicenters of the injured spinal cord. Scale bar, 100 μm. Inset: High-magnification image. Scale bars, 50 μm. The images shown are representative of six mice per time point per group. (H) Quantification of GAP43-positive area (n = 6 mice per group). Wilcoxon rank-sum test: $^*P < 0.05$. Data represent the mean ± s.e.m. (For interpretation of the references to colour in this figure legend, the reader is referred to the web version of this article.)

regenerated axons with injection of β_1 integrin antibodies (Fig. 5G and H). These results suggest that blocking β_1 integrin-dependent recruitment of SAs in the chronic phase may reduce the volume of the glial scar and promote axonal regeneration, which may be a possible route for treating SCI patients in the chronic phase.

4. Discussion

In this study, we found that SAs maintain their morphological features until the chronic phase with a decreased expression of CSPG-related genes compared to the sub-acute phase. Once RAs transformed into SAs, changing the surrounding environment or blocking the integrin-N-cadherin pathway did not significantly alter the morphology or gene expression of SA markers. SAs transplanted into naïve spinal cord formed an astroglial scar with abundant N-cadherin expression and changed the surrounding astrocytes into SAs. Anti-β_1 integrin antibody was able to inhibit the recruitment of SAs and reduce the volume of the glial scar and promote axonal regeneration in the chronic phase of SCI.

The interaction between the β_1 integrin receptors of RAs and type 1 collagen, which is abundant in the damage center, increases the expression of N-cadherin, resulting in SAs. SAs expressed N-cadherin and adhere to each other and form scars (Hara et al., 2017). In the present study, SAs and the glial scar persisted in injured spinal cord until 12 wpi (Fig. 1), suggesting that SAs that emerged in the sub-acute phase survived until the chronic phase and/or that some SAs died due to apoptosis but other SAs were newly recruited from astrocytes in the injured spinal cord. Indeed, we found that SAs could change other astrocytes surrounding them into SAs with abundant N-cadherin expression (Fig. 5). N-cadherin-mediated cell-cell contact inhibits apoptosis in granulosa cells (Peluso et al., 1996). N-cadherin-induced signaling in SAs might also inhibit apoptosis and contribute to the maintenance of the glial scar until the chronic phase. If we can break the N-cadherin bonds formed among SAs, we may be able to manipulate the glial scar by inducing apoptosis of SAs. Trypsin can reversibly degrade N-cadherin bonds (Takeichi, 1977), but when Col-I-SAs were treated with trypsin, they adhered to each other again, with N-cadherins remaining on the surface (Fig. 2D). We treated Col-I-SAs with trypsin and transplanted them into the normal spinal cord, after which SAs did not adopt the phenotype of RAs or NAs, and the expression of N-cadherin did not change. Col-I-SAs that were transplanted into the normal spinal cord formed N-cadherin bonds with neighboring SAs and re-formed the glial scar (Fig. 4B). These results suggest that SAs form glial scars through cell-autonomous regulation. EDTA chelates Ca^{2+} and inhibits N-cadherin adhesion, but this inhibition is reversible. If we can develop a drug that inhibits N-cadherin bonds irreversibly, it may be possible to obtain plasticity of glial scars after degrading glial scars using trypsin.

After SCI, NAs change to RAs, which then gradually transform into SAs *via* the type 1 collagen-β_1 integrin-N-cadherin axis (Hara et al., 2017). RAs are derived from NAs with stimulation of IL-6 or TNF-α. As astrocytes can secrete IL-6 themselves, IL-6 secreted from transplanted SAs can induce phenotypic changes in host NAs to become host RAs (Van Wagoner et al., 1999). Astrocyte can produce collagens *in vitro*, but this expression *in vivo* is suppressed in NAs and RAs (Heck et al., 2003). These data, together with our previous findings from cell specific gene expression analyses using RNA-Seq indicating a relatively low expression of *Col1a1* and *Col1a2* (type 1 collagen), suggest that NAs and RAs *in vivo* might not be able to secrete sufficient type 1 collagen to change RAs to SAs (Hara et al., 2017). Nevertheless, host astrocytes were changed into SAs by transplanted SAs, suggesting that SAs acquire the ability to produce type 1 collagen *in vivo* during the process of phenotypically changing from RAs to SAs.

In the present study, we characterized the molecular biology of the glial scar in the chronic phase of injury. At 12 weeks after SCI, the expression of marker genes of SAs, such as *Sox9*, *Cdh2*, *Slit2*, and *Xylit1*, was maintained at high levels. In contrast, CAs showed a decreased expression of CSPG-related genes compared to SAs (Fig. 1D). Although the expression of CSPGs during acute glial scar formation may contribute to the reduction in the extent of damage, prolonged exposure to CSPGs has a detrimental effect on functional recovery by inhibiting axonal sprouting and remyelination during the chronic phase of SCI (Alizadeh et al., 2019; Pendleton et al., 2013). Therefore, the decreased expression of CSPGs shown in this study indicates that the spinal cord at 12 wpi may be a good environment for axonal regeneration. Indeed, neural stem/precursor cells (NSPCs) transplanted into spinal cord at 4 to 6 wpi did not show axonal growth, but those transplanted at 12 wpi showed an increased expression of *Tubb3*, a marker of axons, suggesting a more suitable environment for axonal growth with the relatively low expression of CSPGs at 12 wpi (Kumamaru et al., 2013).

In conclusion, we demonstrated that scar-forming astrocytes change their phenotype over time depending on the environment surrounding the injured spinal cord. CAs had a higher expression of *Sox9* and lower expression of CSPG-related genes than SAs. Blocking β_1 integrin did not change the phenotype of SAs but did inhibit recruitment of SAs from surrounding astrocytes in the chronic phase of SCI, leading to a reduction in the volume of the glial scar, and promoting axonal regeneration, which may be a possible treatment approach for chronic SCI patients.

Supplementary data to this article can be found online at https://doi.org/10.1016/j.expneurol.2022.114264.

Funding

This work was funded by the General Insurance Association of Japan, ZENKYOREN (National Mutual Insurance Federation of Agricultural Cooperatives), JSPS KAKENHI Grant Number JP19H03771, JP18K16665, JP19K18515, 18 K16680, 22 K09426, 22 K19587, Takeda Science Foundation and AMED under Grant Number JP21gm6210003h9904. The funders had no role in the study design, data collection, data analysis, interpretation, or writing of the report.

Declaration of Competing Interest

The authors declare that they have no known competing financial interests or personal relationships that could have appeared to influence the work reported in this paper.

Data availability

The data that has been used is confidential.

References

Alizadeh, A., Dyck, S.M., Karimi-Abdolrezaee, S., 2019. Traumatic spinal cord injury: an overview of pathophysiology, models and acute injury mechanisms. Front. Neurol. 10, 1–25. https://doi.org/10.3389/fneur.2019.00282.

Anderson, M.A., Burda, J.E., Ren, Y., Ao, Y., O'Shea, T.M., Kawaguchi, R., Coppola, G., Khakh, B.S., Deming, T.J., Sofroniew, M.V., 2016. Astrocyte scar formation AIDS central nervous system axon regeneration. Nature 532, 195–200. https://doi.org/10.1038/nature17623.

Faulkner, J.R., Herrmann, J.E., Woo, M.J., Tansey, K.E., Doan, N.B., Sofroniew, M.V., 2004. Reactive astrocytes protect tissue and preserve function after spinal cord injury. J. Neurosci. 24, 2143–2155. https://doi.org/10.1523/JNEUROSCI.3547-03.2004.

Hara, M., Kobayakawa, K., Ohkawa, Y., Kumamaru, H., Yokota, K., Saito, T., Kijima, K., Yoshizaki, S., Harimaya, K., Nakashima, Y., Okada, S., 2017. Interaction of reactive astrocytes with type I collagen induces astrocytic scar formation through the integrin–N-cadherin pathway after spinal cord injury. Nat. Med. 23, 818–828. https://doi.org/10.1038/nm.4354.

Hasel, P., Liddelow, S.A., 2021. Astrocytes. Curr. Biol. 31 https://doi.org/10.1016/j.cub.2021.01.056. R326–R327.

Heck, N., Garwood, J., Schütte, K., Fawcett, J., Faissner, A., 2003. Astrocytes in culture express fibrillar collagen. Glia 41, 382–392. https://doi.org/10.1002/glia.10184.

Hutson, T.H., Di Giovanni, S., 2019. The translational landscape in spinal cord injury: focus on neuroplasticity and regeneration. Nat. Rev. Neurol. 15, 732–745. https://doi.org/10.1038/s41582-019-0280-3.

Kanemaru, K., Kubota, J., Sekiya, H., Hirose, K., Okubo, Y., Iino, M., 2013. Calcium-dependent N-cadherin up-regulation mediates reactive astrogliosis and neuroprotection after brain injury. Proc. Natl. Acad. Sci. U. S. A. 110, 11612–11617. https://doi.org/10.1073/pnas.1300378110.

Kobayakawa, K., DePetro, K.A., Zhong, H., Pham, B., Hara, M., Harada, A., Nogami, J., Ohkawa, Y., Edgerton, V.R., 2019a. Locomotor training increases synaptic structure with high NGL-2 expression after spinal cord hemisection. Neurorehabil. Neural Repair. https://doi.org/10.1177/1545968319829456.

Kobayakawa, K., Ohkawa, Y., Yoshizaki, S., Tamaru, T., Saito, T., Kijima, K., Yokota, K., Hara, M., Kubota, K., Matsumoto, Y., Harimaya, K., Ozato, K., Masuda, T., Tsuda, M., Tamura, T., Inoue, K., Edgerton, V.R., Iwamoto, Y., Nakashima, Y., Okada, S., 2019b.

Macrophage centripetal migration drives spontaneous healing process after spinal cord injury. Sci. Adv. 5 https://doi.org/10.1126/sciadv.aav5086 eaav5086.
Kumamaru, H., Saiwai, H., Kubota, K., Kobayakawa, K., Yokota, K., Ohkawa, Y., Shiba, K., Iwamoto, Y., Okada, S., 2013. Therapeutic activities of engrafted neural stem/precursor cells are not dormant in the chronically injured spinal cord. Stem Cells 31, 1535–1547. https://doi.org/10.1002/stem.1404.
Liddelow, S.A., Barres, B.A., 2017. Reactive astrocytes: production, function, and therapeutic potential. Immunity 46, 957–967. https://doi.org/10.1016/j.immuni.2017.06.006.
McCarthy, K.D., de Vellis, J., 1980. Preparation of separate astroglial and oligodendroglial cell cultures from rat cerebral tissue. J. Cell Biol. 85, 890–902. https://doi.org/10.1083/jcb.85.3.890.
Mcdonald, J.W., Sadowsky, C., 2002. Spinal-Cord Injury, 359, pp. 417–425.
McKeon, R.J., Schreiber, R.C., Rudge, J.S., Silver, J., 1991. Reduction of neurite outgrowth in a model of glial scarring following CNS injury is correlated with the expression of inhibitory molecules on reactive astrocytes. J. Neurosci. 11, 3398–3411. https://doi.org/10.1523/jneurosci.11-11-03398.1991.
Nathan, F.M., Li, S., 2017. Environmental cues determine the fate of astrocytes after spinal cord injury. Neural Regen. Res. 12, 1964–1970. https://doi.org/10.4103/1673-5374.221144.
Okada, S., Nakamura, M., Katoh, H., Miyao, T., Shimazaki, T., Ishii, K., Yamane, J., Yoshimura, A., Iwamoto, Y., Toyama, Y., Okano, H., 2006. Conditional ablation of Stat3 or Socs3 discloses a dual role for reactive astrocytes after spinal cord injury. Nat. Med. 12, 829–834. https://doi.org/10.1038/nm1425.
Peluso, J.J., Pappalardo, A., Trolice, M.P., 1996. N-cadherin-mediated cell contact inhibits granulosa cell apoptosis in a progesterone-independent manner. Endocrinology 137, 1196–1203.
Pendleton, J.C., Shamblott, M.J., Gary, D.S., Belegu, V., Hurtado, A., Malone, M.L., McDonald, J.W., 2013. Chondroitin sulfate proteoglycans inhibit oligodendrocyte myelination through PTPσ. Exp. Neurol. 247, 113–121. https://doi.org/10.1016/j.expneurol.2013.04.003.
Schildge, S., Bohrer, C., Beck, K., Schachtrup, C., 2013. Isolation and culture of mouse cortical astrocytes. J. Vis. Exp. 1–7 https://doi.org/10.3791/50079.
Shah, P.K., Garcia-Alias, G., Choe, J., Gad, P., Gerasimenko, Y., Tillakaratne, N., Zhong, H., Roy, R.R., Edgerton, V.R., 2013. Use of quadrupedal step training to re-engage spinal interneuronal networks and improve locomotor function after spinal cord injury. Brain 136, 3362–3377. https://doi.org/10.1093/brain/awt265.
Shinozaki, Y., Shibata, K., Yoshida, K., Shigetomi, E., Gachet, C., Ikenaka, K., Tanaka, K. F., Koizumi, S., 2017. Transformation of astrocytes to a neuroprotective phenotype by microglia via P2Y1 receptor downregulation. Cell Rep. 19, 1151–1164. https://doi.org/10.1016/j.celrep.2017.04.047.
Silver, J., Miller, J.H., 2004. Regeneration beyond the glial scar. Nat. Rev. Neurosci. 5, 146–156. https://doi.org/10.1038/nrn1326.
Sofroniew, M.V., 2005. Reactive astrocytes in neural repair and protection. Neuroscientist. 5, 400–407. https://doi.org/10.1177/107385840527832.
Takahashi, S., Watanabe, K., Watanabe, Y., Fujioka, D., Nakamura, T., Nakamura, K., Obata, J.E., Kugiyama, K., 2015. C-type lectin-like domain and fibronectin-like type II domain of phospholipase A2 receptor 1 modulate binding and migratory responses to collagen. FEBS Lett. 589, 829–835. https://doi.org/10.1016/j.febslet.2015.02.016.
Takeichi, M., 1977. Functional correlation between cell adhesive properties and some cell surface proteins. J. Cell Biol. 75, 464–474. https://doi.org/10.1083/jcb.75.2.464.
Tran, A.P., Warren, P.M., Silver, J., 2018. The biology of regeneration failure and success after spinal cord injury. Physiol. Rev. 98, 881–917. https://doi.org/10.1152/physrev.00017.2017.
Van Middendorp, J.J., Hosman, A.J., Donders, A.R.T., Pouw, M.H., Ditunno, J.F., Curt, A., Geurts, A.C., Van De Meent, H., 2011. A clinical prediction rule for ambulation outcomes after traumatic spinal cord injury: a longitudinal cohort study. Lancet 377, 1004–1010. https://doi.org/10.1016/S0140-6736(10)62276-3.
Van Wagoner, N.J., Oh, J.W., Repovic, P., Benveniste, E.N., 1999. Interleukin-6 (IL-6) production by astrocytes: autocrine regulation by IL-6 and the soluble IL-6 receptor. J. Neurosci. 19, 5236–5244. https://doi.org/10.1523/jneurosci.19-13-05236.1999.
Voskuhl, R.R., Peterson, R.S., Song, B., Ao, Y., Morales, L.B.J., Tiwari-Woodruff, S., Sofroniew, M.V., 2009. Reactive astrocytes form scar-like perivascular barriers to leukocytes during adaptive immune inflammation of the CNS. J. Neurosci. 29, 11511–11522. https://doi.org/10.1523/JNEUROSCI.1514-09.2009.
Yoshizaki, S., Kijima, K., Hara, M., Saito, T., Tamaru, T., Tanaka, M., Konno, D.J., Nakashima, Y., Okada, S., 2019. Tranexamic acid reduces heme cytotoxicity via the TLR4/TNF axis and ameliorates functional recovery after spinal cord injury. J. Neuroinflammation 16, 1–15. https://doi.org/10.1186/s12974-019-1536-y.